

Machine Learning Unveils the power law of Finite-Volume Energy Shifts

Wei-Jie Zhang,^{1,2} Zhenyu Zhang,^{1,2,*} Jifeng Hu,^{1,2,†} Bing-Nan Lu,^{3,‡} Jin-Yi Pang,^{4,§} and Qian Wang^{1,2,5,6,¶}

¹*Guangdong-Hong Kong Joint Laboratory of Quantum Matter, Guangdong Provincial Key Laboratory of Nuclear Science, Southern Nuclear Science Computing Center, South China Normal University, Guangzhou 510006, China*

²*Key Laboratory of Atomic and Subatomic Structure and Quantum Control (MOE), Guangdong Basic Research Center of Excellence for Structure and Fundamental Interactions of Matter, Institute of Quantum Matter, South China Normal University, Guangzhou 510006, China*

³*Graduate School of China Academy of Engineering Physics, Beijing 100193, China*

⁴*College of Science, University of Shanghai for Science and Technology, Shanghai 200093, China*

⁵*Southern Center for Nuclear-Science Theory (SCNT), Institute of Modern Physics, Chinese Academy of Sciences, Huizhou 516000, Guangdong Province, China*

⁶*Research Center for Nuclear Physics (RCNP), Osaka University, Ibaraki 567-0047, Japan*

(Dated: March 11, 2025)

Finite-volume extrapolation is an important step for extracting physical observables from lattice calculations. However, it is a significant challenge for the system with long-range interactions. We employ symbolic regression to regress finite-volume extrapolation formula for both short-range and long-range interactions. The regressed formula still holds the exponential form with a factor L^n in front of it. The power decreases with the decreasing range of the force. When the range of the force becomes sufficiently small, the power converges to -1 , recovering the short-range formula as expected. Our work represents a significant advancement in leveraging machine learning to probe uncharted territories within particle physics.

Introduction: Lattice Quantum Chromodynamics, which discretizes space into four dimensional hypercubic lattice and perform the calculation in a given finite volume, is a foundational computational framework for studying strong interaction. It predicts not only the spectrum of conventional hadrons but also reveals the existence of exotic hadronic states. Especially, it provides precise calculations for near-threshold states recently, taking the double charm tetraquark as an example [1–3]. To extract physical observables from lattice calculations, finite-volume extrapolation is essential. However, the presence of long-range interactions presents significant challenges, as they invalidate key assumptions underlying standard approaches, most notably the Lüscher formula [4]. When light particles mediate forces between scattering states, conventional methods may fail, leading to uncontrolled systematic uncertainties. Addressing these issues is crucial for reliable lattice analyses, particularly in systems where long-range effects play a dominant role, such as one-pion exchange in nucleon-nucleon scattering and the effects of light-meson exchange in the D^*D system [5]. Recent theoretical studies [6–9] try to solve this problem by either modifying Lüscher formula numerically, but without explicit formula as simple as that for the short-range interaction [10], or performing quantization conditions using plane wave basis [11]. Moreover, understanding finite-volume effects in two-body systems with long-range interactions is a necessary step toward addressing similar challenges in three-body systems.

Fortunately, deriving fundamental mathematical expressions directly from empirical data [12] is an advantage of symbolic regression [13], which has exhibited its power in physics and scientific research [14]. Unlike traditional regression, it autonomously uncovers interpretable laws by exploring vast expression spaces. This has enabled rediscovery of known physical laws and formulation of novel equations for complex systems [15] even if their underlying principles were elusive. Recent advances in symbolic regression enhance its effectiveness by incorporating physical constraints like dimensional consistency, improving search efficiency and model plausibility. For example, the AI Feynman algorithm, derived 100 equations from the Feynman Lectures on Physics [16]. Its ability to generate human-readable models accelerates discovery across various fields [17, 18]. For instance in high-energy physics, it has revealed fundamental distributions, such as the Tsallis distribution in hadron transverse momentum analysis [19]. Even, it has provided analytical expressions for key low-energy observables, including the Higgs mass, muon anomalous magnetic moment, and dark matter relic density [20].

As the result, we employ symbolic regression to probe the finite-volume extrapolation formula for long-range interactions. Before symbolic regression, we need to prepare samples for training symbolic regression. For these samples, we borrow the Hadron Lattice Effective Field Theory (HLEFT) [21], which is analogous to the Nuclear Lattice Effective Field Theory (NLEFT), a powerful computational framework for *ab initio* nuclear structure calculations [22]. The approach implements a systematic discretization of nucleon-nucleon interactions on a three-dimensional cubic lattice with periodic boundary conditions. These quantum many-body systems are subsequently solved using advanced numerical techniques in-

* Co-first author

† hujf@m.scnu.edu.cn

‡ bnlv@giscaep.ac.cn

§ jypang@usst.edu.cn

¶ qianwang@m.scnu.edu.cn, corresponding author

cluding the Lanczos diagonalization method and auxiliary field Monte Carlo simulations. NLEFT has demonstrated remarkable success across diverse domains of nuclear physics, particularly in characterizing nuclear ground states [23–29] and excited states [30–33], elucidating nuclear intrinsic density distributions and clustering phenomena [34–38], analyzing nucleus-nucleus scattering processes [39, 40], and investigating both zero- and finite-temperature nuclear matter properties [41–44]. The framework has also been effectively extended to study hypernuclear systems [21, 45–47]. However, the presence of finite-volume effects remains a significant challenge in extending NLEFT applications to critical nuclear systems such as the neutron-rich ${}^6\text{He}$ isotope, where the delicate balance of nuclear binding requires exceptional precision. This is another motivation of this work. According to the statement above, our workflow is presented in Fig. 1.

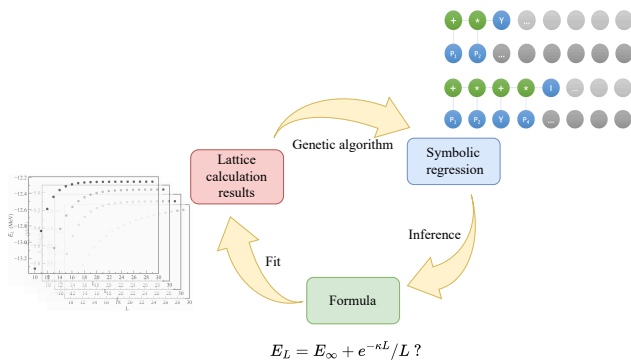


FIG. 1: Workflow of using SR, LEFT and formula.

Samples generation: The HLEFT is used to generate the model-independent samples of two identical boson systems. These samples are fed to Symbolic Regression (SR), which is based on genetic algorithms (GA) [48, 49]. GA allows computer to use fewer prior assumptions and more flexible search space to find final expression. Similar to the evolutionary processes in nature, GA employs mechanisms such as mutations and crossovers to generate new solutions. In this work, the famous PySR, which is a multi-population evolutionary with multiple evolutions performed asynchronously. It uses a classic evolutionary algorithm for every cycle and tournament selection for individual selection. The details of the setup in PySR can be found in Ref. [50].

The challenge for finite volume extrapolation is for long-range interactions [6–9, 11], especially when the range of force is comparable with the box size. Luckily, the extrapolation formula for the short-range potential can be obtained from Lüscher’s formula for $\kappa L \gg 1$ [10], with κ the binding momentum and L the box size. Firstly, we regress the extrapolation formula for the short-range potential as a benchmark for the applicability of PySR model. We work in non-relativistic framework and consider two identical spinless particles with

the same mass $m = 1969$ MeV.¹ The short-range potential in coordinate space reads as

$$V(\mathbf{r}) = -C_0 \delta^3(\mathbf{r}). \quad (1)$$

Here, \mathbf{r} is the relative distance between the two particles. C_0 is the strength of the potential for tuning the binding energy of the two-particle system. The minus sign means an attractive potential. From effective field theory (EFT) point of view, the short-range potential $V(\mathbf{r})$ needs a physical cutoff to isolate the long-range contribution from the short one. Usually, a single-particle regulator [51] $f(\mathbf{p}_1^{(i)}, \mathbf{p}_2^{(i)}) = \prod_{i=1}^2 g_\Lambda(\mathbf{p}_i) g_\Lambda(\mathbf{p}_i')$ is applied, where $g_\Lambda(\mathbf{p}) = \exp(-\mathbf{p}^6/2\Lambda^6)$ is a soft cutoff function with \mathbf{p}_i and \mathbf{p}_i' the momenta of the incoming and outgoing of the i th particle [21]. Thus, the Hamiltonian can be written as:

$$H = \sum_{i=1}^2 \frac{\mathbf{p}_i^2}{2m_i} + f(\mathbf{p}_1^{(i)}, \mathbf{p}_2^{(i)}) V(\mathbf{q}). \quad (2)$$

Here, m_i is the mass of the i th particle. $\mathbf{q} = \mathbf{p} - \mathbf{p}'$ is transferred momentum of the two particles and $\mathbf{p}(\mathbf{p}')$ represents relative incoming (outgoing) momentum between $\mathbf{p}_1(\mathbf{p}_1')$ and $\mathbf{p}_2(\mathbf{p}_2')$. The corresponding potential in momentum space $V(\mathbf{q}) = -C_0$ can be obtained by a Fourier transform from the expression in coordinate space.

The Schrödinger equation is written as:

$$H_L \psi = E_L \psi, \quad (3)$$

H_L and E_L are the Hamiltonian and the binding energy in a cubic box L^3 . The solution of the Schrödinger equation (Eq. 3) can be written explicitly in a single-particle basis $|\psi\rangle = |n_1, \dots, n_N\rangle$ [42], where n_i is an integer triplet specifying the lattice coordinates. The matrix exact diagonalization scheme uses the implicitly restarted Lanczos method to find the eigenvalues and eigenvectors [52] by SciPy [53] in Python. In order to study the finite volume extrapolation formula for short-range potential, we perform simulations on box size $L^3 = 10^3, 11^3, \dots, 30^3$ fm³ cubic lattice with two identical particles. The potential strength C_0 is set to 1.5, 2.0, 2.5 and 3.0 MeV⁻² to generate the samples. With this setup, we can extract the energy E_L in finite volume by solving Eq. (3) for various cases. The details of the samples can be found in Ref. [50].

The Yukawa potential [6]

$$V(\mathbf{r}) = -C_{01} \delta^3(\mathbf{r}) - C_{02} \frac{e^{-\mu r}}{r}. \quad (4)$$

with $1/\mu$ reflecting the range of the force is used to describe the long-range potential. Here, C_{01} and C_{02} are

¹ The polarization of non-zero spin particles would modify the finite-volume extrapolation formula, which will not be discussed in this manuscript.

the strengths of the short-range potential (δ -potential) and the long-range potential (Yukawa potential). One notice that the short-range behavior of Yukawa potential is divergent and needs regularization, which is the reason why the first term exists. For simplicity, we set $C_{01} = C_{02}$ and choose the values 0.03, 0.09, 0.12 and 0.21 MeV^{-2} to generate the samples. These values allow the binding energy of the two-body system with the long-range potential close to that with only the short-range potential. Only in this case, one can isolate the role of the long-range potential on the finite-volume extrapolation formula. For the short-range term, the single-particle regulator $f(\mathbf{p}_1^{(i)}, \mathbf{p}_2^{(i)})$ is still applied. At the same time, for the long-range potential term, the regulator² $\hat{f}(\mathbf{q}) = \exp(-(\mathbf{q}^2 + \mu^2)/\Lambda^2)$ is applied [5]. The Hamilton H in this case can be written as:

$$H = \sum_{i=1}^2 \frac{\mathbf{p}_i^2}{2m_i} + f(\mathbf{p}_1^{(i)}, \mathbf{p}_2^{(i)})V_S(\mathbf{q}) + \hat{f}(\mathbf{q})V_L(\mathbf{q}). \quad (5)$$

Here, both the short-range potential $V_S(\mathbf{q}) = -C_{01}$ and the long-range potential $V_L(\mathbf{q}) \sim \frac{1}{q^2 + \mu^2}$ can be transformed into their coordinate form by Fourier transforms. We perform simulations on box size $L^3 = 10^3, 11^3, \dots, 30^3$ fm³ cubic lattice. The potential strength $C_{01} = C_{02} = 0.03, 0.09, 0.12, 0.21$ MeV^{-2} to obtain binding energies similar to those for only the short-range potential. The details can be found in Ref. [50].

Symbolic regression: We perform symbolic regression on the generated samples that characterize finite-volume effects. The PySR [54] model samples the space of analytic expressions defined by the sign of operators, input variables, and constant terms for minimization through genetic programming. The pool of operations are addition, subtraction, multiplication, division, exponential, logarithm and square, etc. The input variable is box size L . Unlike massive data used in deep learning, a few samples should be sufficient in PySR model. Model evolution progress employs several mechanisms, such as mutations and crossovers, to generate new expressions. We mutate over 50 iterations of 50 different population samples, with each population containing 35 individuals. There are two elements to measure the goodness of the output formula in PySR model, i.e. loss and score. The value of loss is used to measure how well the output formula describes the samples, which is defined as mean square error:

$$\text{Loss} = \sum_{i=1}^N (E_{\text{PySR}}(L_i) - E_L(L_i))^2 / N. \quad (6)$$

Here, $E_{\text{PySR}}(L)$ is the output formula of PySR model, $E_L(L)$ is the energy at box size L^3 calculated from LEFT.

Score is used to estimate the form of the formula, which rewards minimal value of loss and penalizes the more complicated formula. It can be defined as:

$$\text{Score} = -\frac{\Delta \ln(\text{Loss})}{\Delta C}. \quad (7)$$

Here, C is the complexity³ (its values can be found in Ref. [50]), which is defined as the total numbers of operations, variables, and constants used in a formula. PySR model will consider both score, i.e. complexity and loss, to choose the best formula. The other parameters used in training process can be found in Ref. [50].

The training process of SR is very similar to biological population inheritance. In initialization, PySR model randomly provides several kinds of evolutionary frameworks, which are different from each other and are used as a starting point for a given evolution. Mutations and crossovers are throughout each iteration. During each iteration, formulae will be produced and PySR model will choose a best formula into the next iteration according to the value of loss and score. The iterations will stop as long as the loss and complexity are up to the specified value set at the beginning. During this process, the PySR model will choose the best formula throughout iterations.

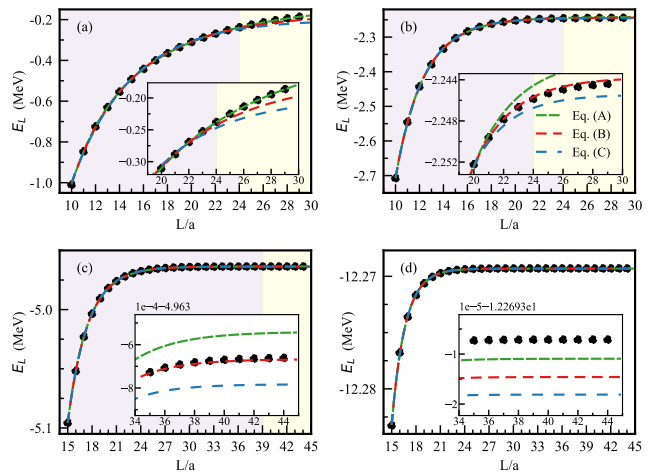


FIG. 2: The results of fitting the formula to samples. (a) is the case of $C_0 = 1.5$ MeV^{-2} , (b) is the case of $C_0 = 2.0$ MeV^{-2} , (c) is the case of $C_0 = 2.5$ MeV^{-2} and (d) is the case of $C_0 = 3.0$ MeV^{-2} . Eqs. (A), (B) and (C) correspond to Eqs. (8A), (8B) and (8C), respectively. The box size L ranges from 10 to 30 fm. The purple region and the yellow region indicate the fitted and predicted area by Eqs. (A), (B) and (C), respectively. Each graph has its own sub-graph to show more detailed of lines between fitted and predicted area.

² Here, Λ is the cutoff to regularize the long-range potential, which is set equal to that for the short-range one above.

³ The upper limit of the C value can be set larger to allow higher order contribution as that in analytic analysis [10].

Results: Based on the PySR model, we can perform a symbolic regression for the samples of the short-range attractive potential to find an expression that uniformly describes the finite-volume extrapolation. In the four cases of C_0 values, three formulae⁴ are accepted by PySR model, as follows,

$$E_L = C_1 + C_2 e^{-C_3 L} / L^2, \quad (8A)$$

$$E_L = C_1 + C_2 e^{-C_3 L} / L, \quad (8B)$$

$$E_L = C_1 + C_2 e^{-C_3 L}. \quad (8C)$$

In Fig. 2, we show the results of the three formulae fitting to the samples with the short-range potential, generated from LEFT. The purple area is the fitting region with the formulae derived from PySR model. The yellow area is the predicted one. For the shallow bound state, i.e. Fig. 2 (a), Eq. (8A) is the best choice. However, the volume size is not big enough to see the convergent behavior, making the regressed formula not universal. When binding energy increases to a few MeV, i.e. Fig. 2 (b) and (c), Eq. (8B) is better than Eq. (8A). When binding energy further increases to more than 10 MeV, i.e. Fig. 2 (d), all the three formulae are good choices because their loss values are much smaller than the other subfigures of Fig. 2. As the result, we conclude that Eq. (8B) is the best regressed uniform formula to describe the samples with a few MeV binding energy.

The current well-established theoretical works [4, 55–57] are based on the Lüscher formula [10] for the short-range potential with $\kappa L \gg 1$ and κ is the binding momentum of the two-body system. The energy shift of a shallow two-body bound state of identical bosons in finite volume is

$$E_L = E_\infty + \frac{C'}{L} \exp(-\kappa L), \quad (9)$$

with C' is the free parameter. This formula is exactly the form of Eq. (8B) regressed by PySR. In addition, the fitted values of the parameter C_3 in Eq. (8B) for the last three cases of Fig. 2 equal to the binding momentum κ numerically. This also demonstrates that we have successfully regressed the finite-volume extrapolation formula for short-range potential.

For the long-range potential, the strengths of the attractive potentials are set to obtain similar binding energies for the short-range potential. The range of the force parameter μ is set as $\mu = 20$ MeV for these four cases. The other values of this parameter and their effect on the finite-volume extrapolation will be discussed afterwards.

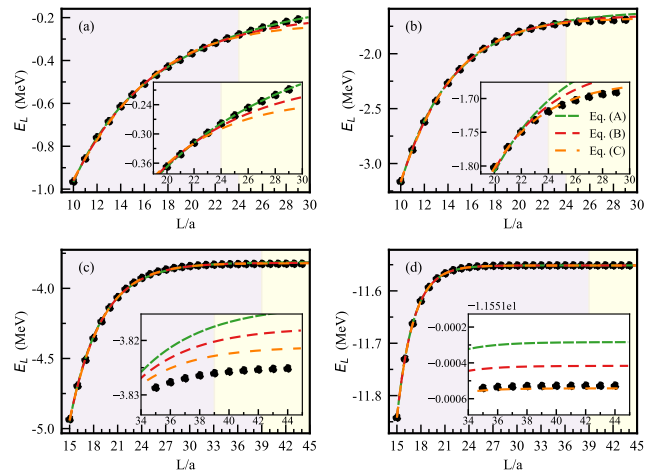


FIG. 3: The results of Eq. (10A) (green short dashed curves), Eq. (10B) (red dashed curves) and Eq. (10C) (orange long dashed curves) fitting to the samples of the long-range potentials with $C_{01} = C_{02} = 0.03$ MeV⁻² (a), $C_{01} = C_{02} = 0.09$ MeV⁻² (b), $C_{01} = C_{02} = 0.12$ MeV⁻² (c), and $C_{01} = C_{02} = 0.21$ MeV⁻² (d). The box size L ranges from 10 ~ 30 fm. The purple region and the yellow region indicate the fitted and predicted area. Each graph has its own sub-graph to show more details around the boundary between fitted and predicted area. The black points are the samples generated from LEFT.

The following three formulae⁵

$$E_L = C_1 + C_2 e^{-C_3 L} / L, \quad (10A)$$

$$E_L = C_1 + C_2 e^{-C_3 L}, \quad (10B)$$

$$E_L = C_1 + C_2 e^{-C_3 L} L. \quad (10C)$$

are accepted by PySR model. Fig. 3 shows the fitting results of the above three formulae to the energy with the long-range interaction. For the case with binding energy smaller than 1 MeV, i.e. Fig. 3(a), Eq. (10A) is preferred. However the binding energy is too small to make the energy convergent in box size 30^3 fm³, making Eq. (10A) unapplicable to other cases. For the other cases, Eq. (10C) describes the samples very well and can be considered as the uniform formulae to describe the energy shift with the the range of the potential as large as 10 fm. In comparison with the formula for the short-range potential, the power of L in front of the exponential becomes larger. This enlighten us that the power of L has a correlation with the range of the force. A theoretical formulation of the two-body quantization condition in the presence of a long-range force was proposed

⁴ For the case of $C_0 = 1.5$ MeV⁻², PySR model gives the formula $E_L = C'_1 + C'_2/L + C'_3/L^2$. For the purpose of uniformity of the formula, when the ratio C'_2/C'_3 is small enough, the formula is approximated as $E_L = C_1 + C_2 e^{-C_3 L} / L^2$.

⁵ For the case of $C_{01} = C_{02} = 0.03$ MeV⁻², PySR model gets the formula $E_L = C'_1 + C'_2/L + C'_3 L$. For the purpose of a uniform form of the formula, when the ratio C'_3/C'_2 is small enough, the formula is approximated as $E_L = C_1 + C_2 e^{-C_3 L} / L$.

in [6–9, 11]. We expect that a comparable power-law dependence on L can be obtained within the improved Lüscher formula.

As discussed above, the power of L in front of the exponential is related to the range of the force. Accordingly, we study tendency of this power in the following. According to the results from machine learning approach, the formula can be written as a general form:

$$E_L = C_1 + C_2 e^{-C_3 L} L^n. \quad (11)$$

Here, n is an unknown parameter and needed to be fixed for various samples. The parameter μ in Eq. (4) is set as 10, 20, ..., 120, 400, 600, 800 MeV corresponding the range of force 19.73, 9.87, ..., 1.64, 0.49, 0.33, 0.25 fm. The first two ranges of force are compatible with the box size. As analyzed in Ref. [50], the power of L in Eq. (11) decreases when the force range decreases. Moreover, when μ goes to infinity, i.e. the short-range interaction, the power n comes back to the formula $E_L = C_1 + C_2 \exp(-C_3 L) L^{-1}$ deduced from the Lüscher formula [10]. It indicates that no matter the form of the potential, the finite-volume extrapolation formula $E_L = C_1 + C_2 \exp(-C_3 L) L^{-1}$ can be reproduced, once the range of force is short enough. On the other hand, when μ goes to zero, the power goes to infinity, which presents the behavior for the infinity long-range interaction [50]. The range of the force for the first two points of Fig.2 in Ref. [50] are compatible with the box size and cannot reflect the correct finite-volume behavior.

Summary and outlook Finite-volume extrapolation is an important step for extracting physical observables from lattice calculations. However, it is a significant chal-

lenge for the system with long-range interactions, especially when the range of the force is comparable with the lattice box size. Several theoretical works have been put forward to extract the finite-volume extrapolation formula based on the modified Lüscher formula numerically. To obtain an exact extrapolation formula, we employ symbolic regression for both short-range and long-range interactions. The samples are generated by the HLEFT and are fed to symbolic regression. As a benchmark, the finite-volume extrapolation formula for short-range interaction has been successfully regressed, i.e. the exponential form $\exp(-\kappa L)$ with the L^{-1} factor in front of it, which is in a good agreement with the theoretical result. Furthermore, we turn to the case of long-range interactions. The regressed results still keep the exponential form, but with the power of L dependent on the range of the force, i.e. the power of L decreases with the decreasing range of the force. When the range of the force becomes sufficiently small, the power converges to -1 , recovering the short-range formula as expected. This agreement further validates the correctness of our extrapolation formula for long-range forces. Our work represents a significant advancement in leveraging machine learning to probe uncharted territories within particle physics.

Acknowledgments: We thank Serdar Elhatisari, Feng-Kun Guo, Ulf-G. Meißner, Andreas Nogga, Akaki G. Rusetsky for their useful discussions on the finite volume dependence from the theoretical side. This work is supported in partly by the NSFC under Grants Nos. 12375072, 12375073, 12275259, and 12135011. The work of Q.W. is also supported by Guangdong Provincial funding under Grant No. 2019QN01X172. B.N. Lu is also supported by NSAF No.U2330401.

-
- [1] M. Padmanath and S. Prelovsek, Signature of a doubly charm tetraquark pole in DD^* scattering on the lattice, Phys. Rev. Lett. **129**, 032002 (2022), arXiv:2202.10110 [hep-lat].
 - [2] S. Chen, C. Shi, Y. Chen, M. Gong, Z. Liu, W. Sun, and R. Zhang, $T_{cc}^+(3875)$ relevant DD^* scattering from $N_f = 2$ lattice QCD, Phys. Lett. B **833**, 137391 (2022), arXiv:2206.06185 [hep-lat].
 - [3] Y. Lyu, S. Aoki, T. Doi, T. Hatsuda, Y. Ikeda, and J. Meng, Doubly charmed tetraquark T_{cc}^+ from Lattice QCD near physical point, Phys. Rev. Lett. **131**, 161901 (2023), arXiv:2302.04505 [hep-lat].
 - [4] M. Lüscher, Volume dependence of the energy spectrum in massive quantum field theories. 2. scattering states, Commun. Math. Phys. **105**, 153 (1986).
 - [5] L. Meng, V. Baru, E. Epelbaum, A. A. Filin, and A. M. Gasparyan, Solving the left-hand cut problem in lattice QCD: $T_{cc}(3875)^+$ from finite volume energy levels, Phys. Rev. D **109**, L071506 (2024), arXiv:2312.01930 [hep-lat].
 - [6] R. Bubna, H.-W. Hammer, F. Müller, J.-Y. Pang, A. Rusetsky, and J.-J. Wu, Lüscher equation with long-range forces, JHEP **05**, 168, arXiv:2402.12985 [hep-lat].
 - [7] S. M. Dawid, F. Romero-López, and S. R. Sharpe, Finite- and infinite-volume study of $DD\pi$ scattering, JHEP **01**, 060, arXiv:2409.17059 [hep-lat].
 - [8] F. Romero-López, A. Rusetsky, N. Schlage, and C. Urbach, Relativistic N -particle energy shift in finite volume, JHEP **02**, 060, arXiv:2010.11715 [hep-lat].
 - [9] T. Iritani, S. Aoki, T. Doi, T. Hatsuda, Y. Ikeda, T. Inoue, N. Ishii, H. Nemura, and K. Sasaki (HAL QCD), Consistency between Lüscher's finite volume method and HAL QCD method for two-baryon systems in lattice QCD, JHEP **03**, 007, arXiv:1812.08539 [hep-lat].
 - [10] M. Lüscher, Volume dependence of the energy spectrum in massive quantum field theories. 1. stable particle states, Commun. Math. Phys. **104**, 177 (1986).
 - [11] L. Meng and E. Epelbaum, Two-particle scattering from finite-volume quantization conditions using the plane wave basis, JHEP **10**, 051, arXiv:2108.02709 [hep-lat].
 - [12] M. Schmidt and H. Lipson, Distilling free-form natural laws from experimental data, Science **324**, 81 (2009).
 - [13] J. R. Koza, Genetic programming: On the programming of computers by means of natural selection (MIT Press,

- Cambridge, MA, USA, 1992).
- [14] N. M. Amil, N. Bredeche, C. Gagné, S. Gelly, M. Schoenauer, and O. Teytaud, A statistical learning perspective of genetic programming, in *Genetic Programming*, edited by L. Vanneschi, S. Gustafson, A. Moraglio, I. De Falco, and M. Ebner (Springer, Berlin, Heidelberg, 2009) pp. 327–338.
- [15] M. Cranmer, A. Sanchez-Gonzalez, P. Battaglia, R. Xu, K. Cranmer, D. Spergel, and S. Ho, Discovering symbolic models from deep learning with inductive biases, (2020), arXiv:2006.11287 [cs.LG].
- [16] S.-M. Udrescu and M. Tegmark, AI Feynman: A physics-inspired method for symbolic regression, *Sci. Adv.* **6**, eaay2631 (2020), arXiv:1905.11481 [physics.comp-ph].
- [17] W. Tenachi, R. Ibata, and F. I. Diakogiannis, Deep symbolic regression for physics guided by units constraints: Toward the automated discovery of physical laws, *The Astrophysical Journal* **959**, 99 (2023).
- [18] Z. Dong, K. Kong, K. T. Matchev, and K. Matcheva, Is the machine smarter than the theorist: Deriving formulas for particle kinematics with symbolic regression, *Phys. Rev. D* **107**, 055018 (2023), arXiv:2211.08420 [hep-ph].
- [19] N. Makke and S. Chawla, Data-driven discovery of Tsallis-like distribution using symbolic regression in high-energy physics, *PNAS Nexus* **3**, pgae467 (2024).
- [20] S. AbdusSalam, S. Abel, and M. Crispim Romão, Symbolic regression for beyond the standard model physics, *Phys. Rev. D* **111**, 015022 (2025), arXiv:2405.18471 [hep-ph].
- [21] Z. Zhang, X.-Y. Hu, G. He, J. Liu, J.-A. Shi, B.-N. Lu, and Q. Wang, Binding of the three-hadron DD^*K system from the lattice effective field theory, *Phys. Rev. D* **111**, 036002 (2025), arXiv:2409.01325 [hep-ph].
- [22] D. Lee, Lattice simulations for few- and many-body systems, *Prog. Part. Nucl. Phys.* **63**, 117 (2009), arXiv:0804.3501 [nucl-th].
- [23] B. Borasoy, E. Epelbaum, H. Krebs, D. Lee, and U.-G. Meißner, Lattice simulations for light nuclei: Chiral effective field theory at leading order, *Eur. Phys. J. A* **31**, 105 (2007), arXiv:nucl-th/0611087.
- [24] E. Epelbaum, H. Krebs, D. Lee, and U.-G. Meißner, Lattice effective field theory calculations for $A = 3, 4, 6, 12$ nuclei, *Phys. Rev. Lett.* **104**, 142501 (2010), arXiv:0912.4195 [nucl-th].
- [25] E. Epelbaum, H. Krebs, D. Lee, and U.-G. Meißner, Lattice calculations for $A = 3, 4, 6, 12$ nuclei using chiral effective field theory, *Eur. Phys. J. A* **45**, 335 (2010), arXiv:1003.5697 [nucl-th].
- [26] T. A. Lähde, E. Epelbaum, H. Krebs, D. Lee, U.-G. Meißner, and G. Rupak, Lattice effective field theory for medium-mass nuclei, *Phys. Lett. B* **732**, 110 (2014), arXiv:1311.0477 [nucl-th].
- [27] B.-N. Lu, N. Li, S. Elhatisari, D. Lee, E. Epelbaum, and U.-G. Meißner, Essential elements for nuclear binding, *Phys. Lett. B* **797**, 134863 (2019), arXiv:1812.10928 [nucl-th].
- [28] B.-N. Lu, N. Li, S. Elhatisari, Y.-Z. Ma, D. Lee, and U.-G. Meißner, Perturbative quantum Monte Carlo method for nuclear physics, *Phys. Rev. Lett.* **128**, 242501 (2022), arXiv:2111.14191 [nucl-th].
- [29] S. Elhatisari et al., Wavefunction matching for solving quantum many-body problems, *Nature* **630**, 59 (2024), arXiv:2210.17488 [nucl-th].
- [30] E. Epelbaum, H. Krebs, T. A. Lähde, D. Lee, U.-G. Meißner, and G. Rupak, *Ab initio* calculation of the spectrum and structure of ^{16}O , *Phys. Rev. Lett.* **112**, 102501 (2014), arXiv:1312.7703 [nucl-th].
- [31] S. Shen, S. Elhatisari, T. A. Lähde, D. Lee, B.-N. Lu, and U.-G. Meißner, Emergent geometry and duality in the carbon nucleus, *Nature Commun.* **14**, 2777 (2023), arXiv:2202.13596 [nucl-th].
- [32] U.-G. Meißner, S. Shen, S. Elhatisari, and D. Lee, *Ab initio* calculation of the alpha-particle monopole transition form factor, *Phys. Rev. Lett.* **132**, 062501 (2024), arXiv:2309.01558 [nucl-th].
- [33] S. Shen, S. Elhatisari, D. Lee, U.-G. Meißner, and Z. Ren, *Ab initio* study of the beryllium isotopes ^7Be to ^{12}Be , (2024), arXiv:2411.14935 [nucl-th].
- [34] E. Epelbaum, H. Krebs, D. Lee, and U.-G. Meißner, *Ab initio* calculation of the Hoyle state, *Phys. Rev. Lett.* **106**, 192501 (2011), arXiv:1101.2547 [nucl-th].
- [35] E. Epelbaum, H. Krebs, T. A. Lähde, D. Lee, and U.-G. Meißner, Structure and rotations of the Hoyle state, *Phys. Rev. Lett.* **109**, 252501 (2012), arXiv:1208.1328 [nucl-th].
- [36] E. Epelbaum, H. Krebs, T. A. Lähde, D. Lee, and U.-G. Meißner, Viability of carbon-based life as a function of the light quark mass, *Phys. Rev. Lett.* **110**, 112502 (2013), arXiv:1212.4181 [nucl-th].
- [37] S. Elhatisari, E. Epelbaum, H. Krebs, T. A. Lähde, D. Lee, N. Li, B.-N. Lu, U.-G. Meißner, and G. Rupak, *Ab initio* calculations of the isotopic dependence of nuclear clustering, *Phys. Rev. Lett.* **119**, 222505 (2017), arXiv:1702.05177 [nucl-th].
- [38] S. Zhang, S. Elhatisari, U.-G. Meißner, and S. Shen, Lattice simulation of nucleon distribution and shell closure in the proton-rich nucleus ^{22}Si , (2024), arXiv:2411.17462 [nucl-th].
- [39] S. Bour, H. W. Hammer, D. Lee, and U.-G. Meißner, Benchmark calculations for elastic fermion-dimer scattering, *Phys. Rev. C* **86**, 034003 (2012), arXiv:1206.1765 [nucl-th].
- [40] S. Elhatisari, D. Lee, G. Rupak, E. Epelbaum, H. Krebs, T. A. Lähde, T. Luu, and U.-G. Meißner, *Ab initio* alpha-alpha scattering, *Nature* **528**, 111 (2015), arXiv:1506.03513 [nucl-th].
- [41] S. Elhatisari et al., Nuclear binding near a quantum phase transition, *Phys. Rev. Lett.* **117**, 132501 (2016), arXiv:1602.04539 [nucl-th].
- [42] B.-N. Lu, N. Li, S. Elhatisari, D. Lee, J. E. Drut, T. A. Lähde, E. Epelbaum, and U.-G. Meißner, *Ab initio* nuclear thermodynamics, *Phys. Rev. Lett.* **125**, 192502 (2020), arXiv:1912.05105 [nucl-th].
- [43] Z. Ren, S. Elhatisari, T. A. Lähde, D. Lee, and U.-G. Meißner, *Ab initio* study of nuclear clustering in hot dilute nuclear matter, *Phys. Lett. B* **850**, 138463 (2024), arXiv:2305.15037 [nucl-th].
- [44] Y.-Z. Ma, Z. Lin, B.-N. Lu, S. Elhatisari, D. Lee, N. Li, U.-G. Meißner, A. W. Steiner, and Q. Wang, Structure factors for hot neutron matter from *Ab initio* lattice simulations with high-fidelity chiral interactions, *Phys. Rev. Lett.* **132**, 232502 (2024), arXiv:2306.04500 [nucl-th].
- [45] S. Bour, D. Lee, H. W. Hammer, and U.-G. Meißner, *Ab initio* lattice results for fermi polarons in two dimensions, *Phys. Rev. Lett.* **115**, 185301 (2015), arXiv:1412.8175 [cond-mat.quant-gas].
- [46] V. Scarduelli, L. R. Gasques, L. C. Chamon, and A. Lépine-Szily, A method to optimize mass discrimina-

- tion of particles identified in ΔE - E silicon surface barrier detector systems, *Eur. Phys. J. A* **56**, 24 (2020).
- [47] F. Hildenbrand, S. Elhatisari, Z. Ren, and U.-G. Meißner, Towards hypernuclei from nuclear lattice effective field theory, *Eur. Phys. J. A* **60**, 215 (2024), arXiv:2406.17638 [nucl-th].
- [48] D. G. Ireland, S. Janssen, and J. Ryckebusch, A genetic algorithm analysis of N^* resonances in $p(\gamma, K^+)\Lambda$ reactions, *Nucl. Phys. A* **740**, 147 (2004), arXiv:nucl-th/0312103.
- [49] C. Fernández-Ramírez, E. Moya de Guerra, A. Udías, and J. M. Udías, Properties of nucleon resonances by means of a genetic algorithm, *Phys. Rev. C* **77**, 065212 (2008), arXiv:0805.4178 [nucl-th].
- [50] See supplemental material at xxx for the detailed setup of the pysr model, the samples from lattice eft, the details of symbolic regression and some numerical results.
- [51] B.-N. Lu and B.-G. Deng, Renormalization of many-body effective field theory, (2023), arXiv:2308.14559 [nucl-th].
- [52] R. B. Lehoucq, D. C. Sorensen, and C. Yang, Arpack users' guide: Solution of large-scale eigenvalue problems with implicitly restarted arnoldi methods (SIAM, Philadelphia, PA, 1998).
- [53] P. Virtanen et al., SciPy 1.0—fundamental algorithms for scientific computing in Python, *Nature Meth.* **17**, 261 (2020), arXiv:1907.10121 [cs.MS].
- [54] M. Cranmer, Interpretable machine learning for science with pysr and symbolicregression.jl, (2023), arXiv:2305.01582 [astro-ph.IM].
- [55] M. Döring, H. W. Hammer, M. Mai, J. Y. Pang, t. A. Rusetsky, and J. Wu, Three-body spectrum in a finite volume: The role of cubic symmetry, *Phys. Rev. D* **97**, 114508 (2018), arXiv:1802.03362 [hep-lat].
- [56] H.-W. Hammer, J.-Y. Pang, and A. Rusetsky, Three-particle quantization condition in a finite volume: 1. the role of the three-particle force, *JHEP* **09**, 109, arXiv:1706.07700 [hep-lat].
- [57] S. König and D. Lee, Volume dependence of N -body bound states, *Phys. Lett. B* **779**, 9 (2018), arXiv:1701.00279 [hep-lat].

Supplementary Material

Wei-Jie Zhang,^{1,2} Zhenyu Zhang,^{1,2,*} Jifeng Hu,^{1,2,†} Bing-Nan Lu,^{3,‡} Jin-Yi Pang,^{4,§} and Qian Wang^{1,2,5,¶}

¹*Guangdong-Hong Kong Joint Laboratory of Quantum Matter, Guangdong Provincial Key Laboratory of Nuclear Science, Southern Nuclear Science Computing Center, South China Normal University, Guangzhou 510006, China*

²*Key Laboratory of Atomic and Subatomic Structure and Quantum Control (MOE), Guangdong Basic Research Center of Excellence for Structure and Fundamental Interactions of Matter, Institute of Quantum Matter, South China Normal University, Guangzhou 510006, China*

³*Graduate School of China Academy of Engineering Physics, Beijing 100193, China*

⁴*College of Science, University of Shanghai for Science and Technology, Shanghai 200093, China*

⁵*Southern Center for Nuclear-Science Theory (SCNT), Institute of Modern Physics, Chinese Academy of Sciences, Huizhou 516000, Guangdong Province, China*

(Dated: March 11, 2025)

In the supplementary material, we present the details of the PySR model, the intermediate results during the training and some theoretical discussions.

I. THE DETAILS OF THE PYSR MODEL

Lots of parameters, which can be modified to meet requirements, are provided in PySR. Some vital parameters will be introduced below. After one training process, PySR gives one formula as output. During this period, a new equation accompanied by its complexity and loss, is generated in each iteration.

Here, complexity is used to estimate the form of the formula. The more complicated equation, the higher value of complexity. The formula is consisted by constant term, variable term and sign of operators. Thus PySR provides some parameters to modify them. Parameter “complexity_of_constants” is used to modify complexity of the constants in formula and parameter “complexity_of_variables” is used to modify the variables, namely L in the formula. In the training process, “complexity_of_variables” is changed larger than its default value. While “complexity_of_constants” remain default. Sign of operators is used to separate the operators into two kinds of operators. If the operators, such as “+” and “ \times ”, need two elements, it is called binary operator, denoted by “binary_operators”. Besides, if the operators, such as “exp” and “log”, need only one element, it is called unary operator, denoted as “unary_operators”. After carefully considering final results, it is not appropriate to use trigonometric functions to characterize finite volume effect. Thus, parameter “unary_operators” = [“exp”, “sqrt”, “log”] is used. To simplify the result, some complicated forms, such as nested structure, should be prohibited by the parameter “nested_constraints”. Here, we set parameter “nested_constraints” = “exp”:{“exp”:0}, which means the form of nested exponential functions is not allowed.

Except for the complexity, the value of loss also plays an important role in choosing formula. Like most machine learning processes, it is necessary to use loss function to judge which formula is better. Parameter “elementwise_loss” is used to select the loss function in the training period. Usually, mean square error (MSE) is used in machine learning. Thus, “elementwise_loss” = L2DistLoss().

After defining complexity and loss, PySR will select a formula considering two elements mentioned above. Parameter “model_selection” is used to control which formula can be chosen by PySR. Here, we set the “model_selection” = “best”, which means PySR will consider both complexity and loss to choose the best formula.

II. THE SAMPLES FROM LATTICE EFT

In two-body system, considering only short-range potential between two identical particles, we use the Lattice Effective Field Theory (LEFT) to generate the E_L at finite volume for different cases. The detailed data can be found Tab. II. The lattice spacing a should not be set smaller than the typical hadron size, as hadrons are degrees of freedom in LEFT. The spatial lattice spacing is chosen as $a = 1/200(1/300) \text{ MeV}^{-1} \approx 0.99(0.67) \text{ fm}$ for smaller (larger) binding energies. The soft cutoff is chosen $\Lambda = 350(600) \text{ MeV}$ to make sure that it is much larger than

* Co-first author

† hujf@m.scnu.edu.cn

‡ bnlv@giscaep.ac.cn

§ jypang@usst.edu.cn

¶ qianwang@m.scnu.edu.cn, corresponding author

TABLE I: Some parameters and their functions and values in PySR model.

Parameter	Function	Value
populations	determine the number of populations in each generation during evolution	50
population_size	number of the candidate in each population	35
ncycles_per_iteration	number of total mutations to run, per 10 samples of the population, per iteration	550
niterations	number of iterations of the algorithm to run	40
maxsize	upper complexity limit of final result	15
binary_operators	list of strings for binary operators used in the search	“+”, “-”, “*”, “/”
unary_operators	operators which only take a single scalar as input	“exp”, “sqrt”, “log”
nested_constraints	specifies how many times a combination of operators can be nested	“exp”：“exp”:0
complexity_of_variables	global complexity of variables	1
complexity_of_constants	complexity of constants	2
optimizer_iterations	number of iterations that the constants optimizer can take	30
perturbation_factor	constants are perturbed by a max factor of (perturbation_factor*T + 1), either multiplied by this or divided by this	0.076
parsimony	multiplicative factor for how much to punish complexity	0.032
adaptive_parsimony_scaling	weigh of simple formula	20.0
model_selection	select a final expression from the list of best expression at each complexity	“best”
elementwise_loss	elementwise loss function	“L2DistLoss()”

the binding momentum κ and smaller than π/a . To satisfy the requirement of the lattice EFT discussed above, we choose $a = 1/200 \text{ MeV}^{-1}$ and $\Lambda = 350 \text{ MeV}$ for $C_0 = 1.5, 2.0 \text{ MeV}^{-2}$. Those values for $C_0 = 2.5, 3.0 \text{ MeV}^{-2}$ are $a = 1/300 \text{ MeV}^{-1}$ and $\Lambda = 600 \text{ MeV}$. Those setups require minimal computing resources and makes the physics independent on them.

In two-body system, considering both the short-range and the long-range potential between two particles, the LEFT is used to generate the energy E_L in L^3 box for different cases. The range of the force parameter μ in is set as $\mu = 20 \text{ MeV}$. The spatial lattice spacing is chosen as $a = 1/200(1/300) \text{ MeV}^{-1}$ for $C_{01} = C_{02} = 0.03, 0.09 \text{ MeV}^{-2}(0.12, 0.21 \text{ MeV}^{-2})$ corresponding to $\Lambda = 350 \text{ MeV}(600 \text{ MeV})$. More detailed samples can be found in Tab. III.

To study the correlation between the power of L and the range of the force, we generate samples with different ranges of the force. To remove the effect of the binding energy on the value of n , the parameters C_{01} and C_{02} are chosen to produce binding energy around -3.83 MeV . The other parameters are set as $a = 1/300 \text{ MeV}^{-1}$, $\Lambda = 600 \text{ MeV}$ and box size L ranges from $10 \sim 30 \text{ fm}$ (i.e. L/a ranges from 15 to 45). The parameter μ is set as 10, 20, ..., 120, 400, 600, 800 MeV corresponding the range of force 19.73, 9.87, ..., 1.64, 0.49, 0.33, 0.25 fm. The first two ranges of force are compatible with the box size. More specific, in two-body system, considering both short-range and the long-range potential, we generate samples with 15 μ values. The detailed results can be found in Tab. IV.

III. THE DETAILS OF SYMBOLIC REGRESSION

The details of the output formula for each iteration in the PySR model for the short-range potential and the long-range potential are listed in Tab. V and Tab. VI, respectively.

TABLE II: The energy E_L for box size L^3 in different spatial lattice spacings a , cutoff Λ , C_0 , which adjusts the strength of the δ -potential, and L/a . The masses of particles are set as 1969 MeV.

$a(\text{MeV}^{-1})$	1/200	1/200	1/300	1/300		1/200	1/200	1/300	1/300
$\Lambda(\text{MeV})$	350	350	600	600		350	350	600	600
$C_0(\text{MeV}^{-2})$	1.50	2.00	2.50	3.00		1.50	2.00	2.50	3.00
L/a	$E_L(\text{MeV})$				L/a	$E_L(\text{MeV})$			
10	-1.010	-2.708	...		28	-0.194	-2.245	-4.964	-12.269
11	-0.846	-2.545	...		29	-0.186	-2.244	-4.964	-12.269
12	-0.724	-2.443	...		30	...		-4.964	-12.269
13	-0.629	-2.379	...		31	...		-4.964	-12.269
14	-0.553	-2.334	...		32	...		-4.964	-12.269
15	-0.492	-2.303	-5.096	-12.283	33	...		-4.964	-12.269
16	-0.442	-2.284	-5.052	-12.277	34	...		-4.964	-12.269
17	-0.400	-2.271	-5.023	-12.274	35	...		-4.964	-12.269
18	-0.365	-2.262	-5.003	-12.272	36	...		-4.964	-12.269
19	-0.335	-2.256	-4.990	-12.271	37	...		-4.964	-12.269
20	-0.310	-2.252	-4.982	-12.270	38	...		-4.964	-12.269
21	-0.288	-2.250	-4.976	-12.270	39	...		-4.964	-12.269
22	-0.269	-2.248	-4.972	-12.270	40	...		-4.964	-12.269
23	-0.252	-2.247	-4.969	-12.269	41	...		-4.964	-12.269
24	-0.238	-2.245	-4.968	-12.269	42	...		-4.964	-12.269
25	-0.225	-2.246	-4.966	-12.269	43	...		-4.964	-12.269
26	-0.214	-2.245	-4.966	-12.269	44	...		-4.964	-12.269
27	-0.203	-2.245	-4.965	-12.269					

TABLE III: The energy E_L in box size L^3 with different spatial lattice spacings a , cutoff Λ , C_{01} , which adjusts the size of short-range potential, C_{02} , which adjusts the size of long-range potential, and L/a . The masses of the two particles are set as 1969 MeV.

$a(\text{MeV}^{-1})$	1/200	1/200	1/300	1/300		1/200	1/200	1/300	1/300
$\Lambda(\text{MeV})$	350	350	600	600		350	350	600	600
$C_{01}/C_{02}(\text{MeV}^{-2})$	0.03	0.09	0.12	0.21		0.03	0.09	0.12	0.21
L/a	$E_L(\text{MeV})$				L/a	$E_L(\text{MeV})$			
10	-0.965	-3.162	...		28	-0.220	-1.694	-3.856	-11.552
11	-0.857	-2.873	...		29	-0.208	-1.691	-3.848	-11.552
12	-0.758	-2.619	...		30	...		-3.842	-11.552
13	-0.683	-2.430	...		31	...		-3.838	-11.552
14	-0.614	-2.266	...		32	...		-3.834	-11.552
15	-0.559	-2.142	-4.933	-11.842	33	...		-3.832	-11.552
16	-0.509	-2.037	-4.694	-11.730	34	...		-3.830	-11.552
17	-0.467	-1.957	-4.510	-11.662	35	...		-3.829	-11.552
18	-0.429	-1.891	-4.354	-11.619	36	...		-3.828	-11.552
19	-0.397	-1.841	-4.234	-11.593	37	...		-3.827	-11.552
20	-0.367	-1.802	-4.137	-11.576	38	...		-3.826	-11.552
21	-0.342	-1.772	-4.063	-11.566	39	...		-3.826	-11.552
22	-0.318	-1.749	-4.004	-11.561	40	...		-3.826	-11.552
23	-0.298	-1.732	-3.960	-11.557	41	...		-3.826	-11.552
24	-0.279	-1.719	-3.926	-11.555	42	...		-3.825	-11.552
25	-0.262	-1.710	-3.900	-11.554	43	...		-3.825	-11.552
26	-0.247	-1.703	-3.881	-11.553	44	...		-3.825	-11.552
27	-0.233	-1.697	-3.867	-11.552					

IV. THE EFFECT OF RANGE OF THE FORCE ON THE FINITE-VOLUME EXTRAPOLATION

As discussed in the letter, the finite-volume extrapolation formula for both short-range and long-range interactions can be written in a compact form

$$E_L = C_1 + C_2 e^{-C_3 L} L^n. \quad (1)$$

TABLE IV: The energy E_L in L^3 box size with $a = 1/300 \text{ MeV}^{-1}$ and $\Lambda = 600 \text{ MeV}$. The long-range parameter μ is set in the range $[10, 120] \text{ MeV}$.

$\mu(\text{MeV})$	10	20	30	40	50	60	70	80	90	100	110	120
$C_{01}/C_{02}(\text{MeV}^{-2})$	0.107	0.120	0.133	0.147	0.161	0.175	0.191	0.206	0.223	0.240	0.258	0.276
L/a	$E_L(\text{MeV})$											
15	-5.041	-4.933	-4.819	-4.749	-4.667	-4.571	-4.554	-4.470	-4.454	-4.414	-4.390	-4.341
16	-4.800	-4.694	-4.587	-4.527	-4.456	-4.371	-4.366	-4.291	-4.285	-4.253	-4.237	-4.194
17	-4.610	-4.510	-4.410	-4.361	-4.300	-4.224	-4.229	-4.162	-4.164	-4.138	-4.128	-4.090
18	-4.446	-4.354	-4.266	-4.228	-4.178	-4.111	-4.125	-4.065	-4.074	-4.053	-4.048	-4.014
19	-4.317	-4.235	-4.157	-4.130	-4.088	-4.029	-4.050	-3.995	-4.009	-3.993	-3.992	-3.960
20	-4.208	-4.137	-4.070	-4.053	-4.020	-3.967	-3.995	-3.944	-3.962	-3.950	-3.951	-3.921
21	-4.124	-4.063	-4.006	-3.997	-3.971	-3.923	-3.955	-3.907	-3.929	-3.919	-3.922	-3.894
22	-4.054	-4.004	-3.956	-3.955	-3.934	-3.890	-3.926	-3.880	-3.905	-3.896	-3.902	-3.874
23	-4.000	-3.960	-3.919	-3.924	-3.907	-3.866	-3.909	-3.861	-3.888	-3.881	-3.887	-3.860
24	-3.957	-3.926	-3.891	-3.901	-3.888	-3.849	-3.891	-3.848	-3.876	-3.869	-3.877	-3.850
25	-3.924	-3.901	-3.870	-3.885	-3.874	-3.836	-3.880	-3.838	-3.867	-3.861	-3.869	-3.843
26	-3.898	-3.881	-3.855	-3.872	-3.864	-3.828	-3.873	-3.831	-3.861	-3.856	-3.864	-3.838
27	-3.879	-3.867	-3.844	-3.864	-3.856	-3.821	-3.867	-3.826	-3.856	-3.852	-3.860	-3.835
28	-3.863	-3.856	-3.836	-3.857	-3.851	-3.816	-3.863	-3.823	-3.853	-3.849	-3.858	-3.832
29	-3.852	-3.848	-3.830	-3.852	-3.847	-3.813	-3.861	-3.820	-3.851	-3.847	-3.856	-3.830
30	-3.843	-3.842	-3.825	-3.849	-3.844	-3.811	-3.859	-3.818	-3.849	-3.845	-3.854	-3.829
31	-3.837	-3.838	-3.822	-3.847	-3.842	-3.809	-3.857	-3.817	-3.848	-3.844	-3.853	-3.828
32	-3.832	-3.834	-3.820	-3.845	-3.841	-3.808	-3.856	-3.816	-3.847	-3.843	-3.853	-3.827
33	-3.828	-3.832	-3.818	-3.843	-3.840	-3.807	-3.855	-3.815	-3.847	-3.843	-3.852	-3.827
34	-3.825	-3.830	-3.817	-3.842	-3.839	-3.807	-3.855	-3.815	-3.846	-3.842	-3.852	-3.826
35	-3.823	-3.829	-3.816	-3.842	-3.838	-3.806	-3.854	-3.814	-3.846	-3.842	-3.851	-3.826
36	-3.822	-3.828	-3.815	-3.841	-3.838	-3.805	-3.854	-3.814	-3.846	-3.842	-3.851	-3.826
37	-3.821	-3.827	-3.814	-3.841	-3.838	-3.805	-3.854	-3.814	-3.846	-3.842	-3.851	-3.826
38	-3.820	-3.827	-3.814	-3.841	-3.837	-3.805	-3.854	-3.814	-3.846	-3.842	-3.851	-3.826
39	-3.819	-3.826	-3.814	-3.841	-3.837	-3.805	-3.854	-3.814	-3.845	-3.841	-3.851	-3.826
40	-3.818	-3.826	-3.814	-3.840	-3.837	-3.805	-3.854	-3.814	-3.845	-3.841	-3.851	-3.826
41	-3.818	-3.826	-3.813	-3.840	-3.837	-3.805	-3.853	-3.814	-3.845	-3.841	-3.851	-3.826
42	-3.818	-3.825	-3.813	-3.840	-3.837	-3.804	-3.853	-3.814	-3.845	-3.841	-3.851	-3.826
43	-3.818	-3.825	-3.813	-3.840	-3.837	-3.804	-3.853	-3.813	-3.845	-3.841	-3.851	-3.826
44	-3.817	-3.825	-3.813	-3.840	-3.837	-3.804	-3.853	-3.813	-3.845	-3.841	-3.851	-3.826

with the power of L depending on the range of the force. We set the range parameter $\mu = 10, 20, \dots, 120, 400, 600, 800 \text{ MeV}$ corresponding the range of force $19.73, 9.87, \dots, 1.64, 0.49, 0.33, 0.25 \text{ fm}$ to probe the behavior of n . Fig. 1 presents the fitting results for the eight $n = 5/2, 2, 3/2, 1, 1/2, 0, -1/2, -1$ (denoting as Eq.(A), Eq.(B),... Eq.(H) in Fig. 1) values to the energy shift. Here the fitting parameters are the C_1, C_2 and C_3 in Eq. (1). One can see that the n value decreases with the increasing μ . Furthermore, we release the power n as an additional free parameter in the fitting. The behavior of the power n in terms of the range parameter μ is illustrated in Fig. 2. One can see when μ goes to infinity, i.e. the short-range limit, the power n comes back to -1 , recovering the formula

TABLE V: The process of PySR model generates formula with the samples for $a = 1/200 \text{ MeV}^{-1}$, $\Lambda = 350 \text{ MeV}$ and $C_0 = 2.0 \text{ MeV}^{-2}$ short-range potential only. The first column represents the evolution times. The last column is the output formula for each evolution after the simplification. And the bold formula is accepted by PySR model after one cycle.

Times	Complexity	Loss	Score	Equation
1	1	5.818	0.000	L
2	2	0.014	6.016	-2.312
3	4	0.010	0.180	$L - 2.410$
4	5	0.007	0.396	$-2.549 \exp(L)$
5	6	0.005	0.220	$-3.144 \exp(\sqrt{L})$
6	7	0.003	0.653	$(-0.028/L) - 1.992$
7	8	0.003	0.000	$(-0.028/L) - 1.992$
8	9	0.001	0.682	$-0.001/L^2 - 2.148$
9	10	3.679×10^{-4}	1.341	$(\sqrt{L} - 0.171)/L - 3.696$
10	11	1.831×10^{-6}	5.302	$-29.889 \exp(-83.458L) - 2.245$
11	12	1.826×10^{-6}	0.003	$-\exp(-83.388L + 3.393) - 2.245$
12	13	6.333×10^{-7}	1.059	$-0.629 \exp(-66.049L)/L - 2.244$
13	14	6.292×10^{-7}	0.006	$-0.628 \exp(-66.022L)/L - 2.244$

TABLE VI: The process of generating a formula with the samples for $a = 1/200 \text{ MeV}^{-1}$, $\Lambda = 350 \text{ MeV}$ and $C_{01} = C_{02} = 0.09 \text{ MeV}^{-2}$ short-range and long-range potential. The bold formula is accepted by PySR model after one cycle. The last line indicates that, even when the complexity increases, the output formula is not significantly improved.

Times	Complexity	Loss	Score	Equation
1	1	4.660	0.000	L
2	2	0.153	3.418	$\log(L)$
3	4	0.072	0.380	$-0.172/L$
4	5	0.021	1.237	$-0.613/\sqrt{L}$
5	6	0.008	1.006	$-\exp(0.058/L)$
6	8	0.002	0.676	$-\exp(0.056/L) - L$
7	9	0.002	0.253	$-0.004/L^2 - 1.413$
8	11	5.672×10^{-5}	1.646	$-15.311/\exp(46.272L) - 1.661$
9	13	6.928×10^{-6}	1.051	$-695.626L/\exp(63.072L) - 1.677$
10	15	6.571×10^{-6}	0.026	$-681.508L/\exp(62.467L) + L^2 - 1.660$

$E_L = C_1 + C_2 \exp(-C_3 L)L^{-1}$ deduced from the Lüscher formula for the short-range interaction. On the other hand, when μ goes to zero, the power goes to infinity, which presents the behavior for the infinity long-range interaction. The flat behavior of the first two points is limited by our box size. In this case, we also present the dependence of the parameter C_3 on the range parameter μ in Fig. 3. The value of C_3 goes to the binding momentum for short-range interaction, i.e. for infinity μ value.

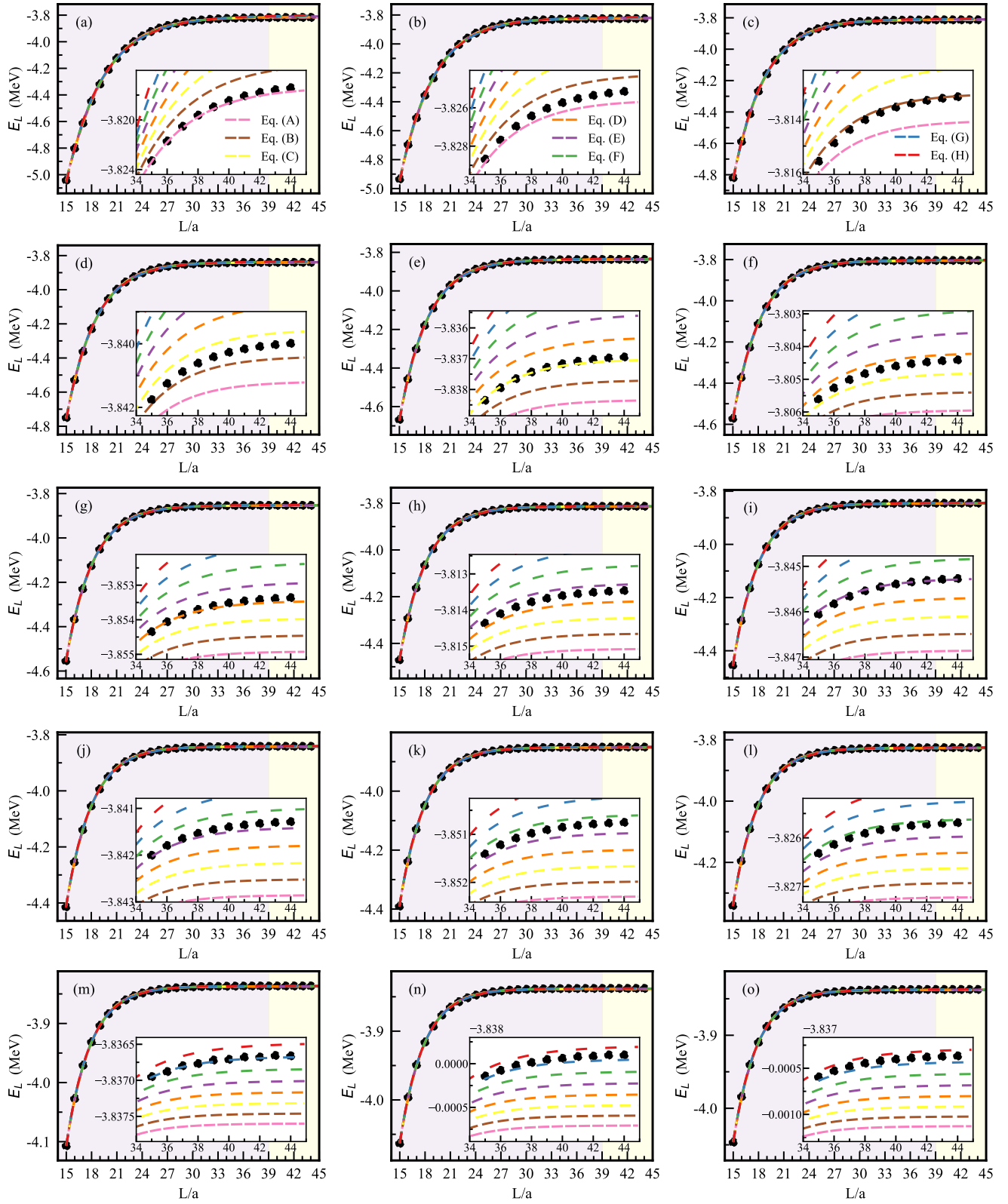


FIG. 1: The fitting results of $E_L = C_1 + C_2 e^{-C_3 L} L^n$ to samples with the long-range parameter $\mu = 10, 20, \dots, 120, 400, 600, 800$ MeV denoted from (a) to (o) in order. For all the cases, the binding energy is around 3.83 MeV and the parameters $a = 1/300$ MeV $^{-1}$, $\Lambda = 600$ MeV. The eight lines, i.e. pink, brown, yellow, orange, purple, green, blue and red lines, represent the power $n = 5/2, 2, 3/2, 1, 1/2, 0, -1/2, -1$ of L from bottom to top in each figure. The black dots are the samples generated by LEFT for various cases.

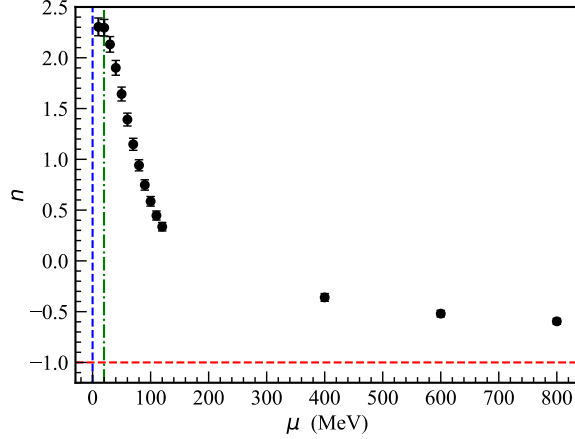


FIG. 2: The dependence of the power n in Eq. (1) on the range parameter μ . The vertical blue dashed line is the infinity long-range limit. The vertical green dot-dashed line corresponds to the lower limit of our box size, i.e. $\frac{\hbar c}{10 \text{ fm}}$. The horizontal red dashed line is the short-range value -1 from Lüscher formula, which is also the convergent value for infinity large μ . The behavior presents very good short-range and long-range behaviors.

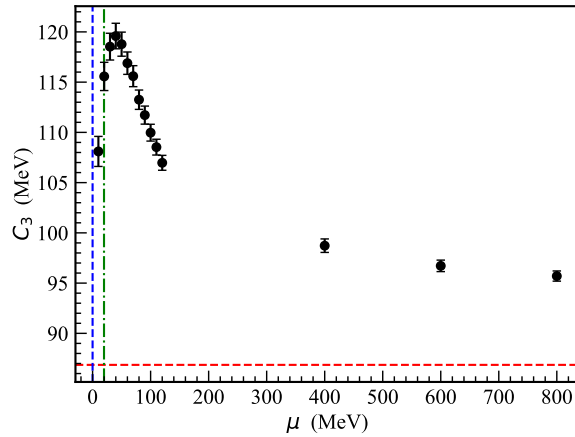


FIG. 3: The dependence of the parameter C_3 on the range parameter μ with the power n corresponding to the results of Fig. 2. The vertical blue dashed line is the infinity long-range limit. The vertical green dot-dashed line corresponds to the lower limit of our box size, i.e. $\frac{\hbar c}{10 \text{ fm}}$. The horizontal red dashed line is the binding momentum $\kappa = \sqrt{mE_\infty}$, which is also the convergent value for infinity large μ .